Unlocking the Potential of Internal Li-ion transfer in Ni-Rich Cathodes Blended with $LiFePO_4$ to Address First Cycle Irreversible Capacity Loss and Degradation

Myoungsoo Kang[1], Seheon Oh[1], Kangwoo Ahn[3], Hyun Woo Kim[4], Jin Bae Lee[5], Jeongsik Yun[6], Minkyu Kim[1,2]*

[1]Department of Chemistry and Chemical Engineering, Inha University, 100 Inha-ro, Michuhol-gu, Incheon, 22212, Republic of Korea

[2]Department of Chemistry, Inha University, 100 Inha-ro, Michuhol-gu, Incheon, 22212, Republic of Korea

[3]Pohang Accelerator Laboratory (PAL), Pohang University of Science and Technology (POSTECH), Pohang, Gyeongbuk 37673, Republic of Korea

[4]Department of Chemical Engineering, Gyeongsang National University, Jinju 52828, Republic of Korea

[5]Research Center for Materials Analysis, Korea Basic Science Institute (KBSI), 169-148 Gwahak-ro Yuseong-gu, Daejeon 34133, Republic of Korea

[6]Department of Energy and Chemical Engineering, Innovation Center for Chemical Engineering, Incheon National University, 119 Academy-ro, Yeonsu-gu, Incheon, 22012 Republic of Korea

*Corresponding Author: minkyu.kim@inha.ac.kr (Minkyu Kim)

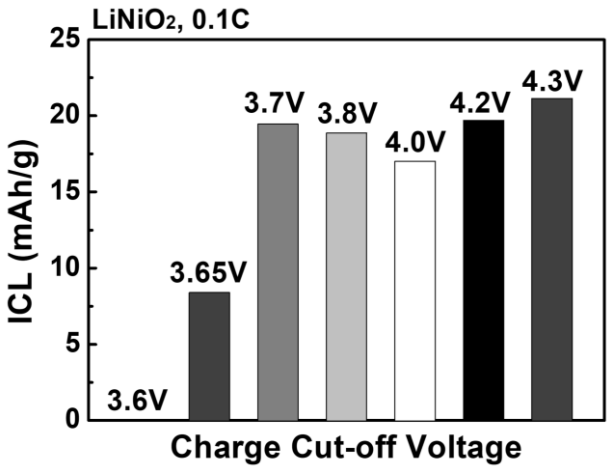

Fig. S1. ICL values of $LiNiO_2$ at 0.1C depending on upper cutoff voltage (3.6 V, 3.65 V, 3.7 V, 3.8 V, 4.0 V, 4.2 V, 4.3 V) while the lower cutoff voltage was fixed at 3.0 V. This test was conducted using different cells for each upper cutoff voltage.

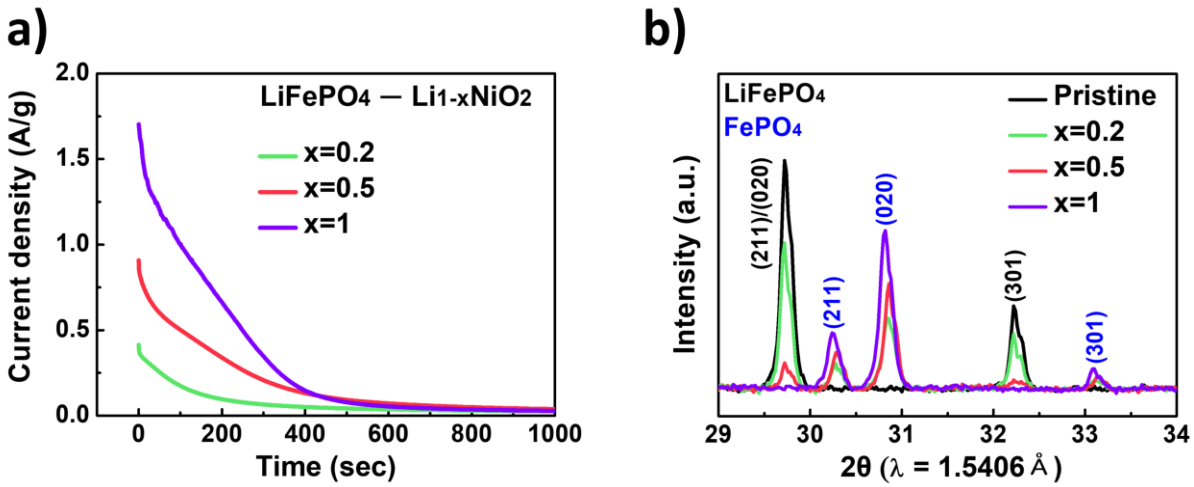

Fig. S2. a) Current density *vs.* time curves for short-circuited $LiFePO_4$ and electrochemically delithiated $Li_{1-x}NiO_2$ electrodes (x = 0.2, 0.5, 1). b) X-ray diffraction (XRD) patterns of $LiFePO_4$ electrodes after being short-circuited with $Li_{1-x}NiO_2$ electrodes (x = 0.2, 0.5, 1), shown at selected 2θ regions (29° - 34°).

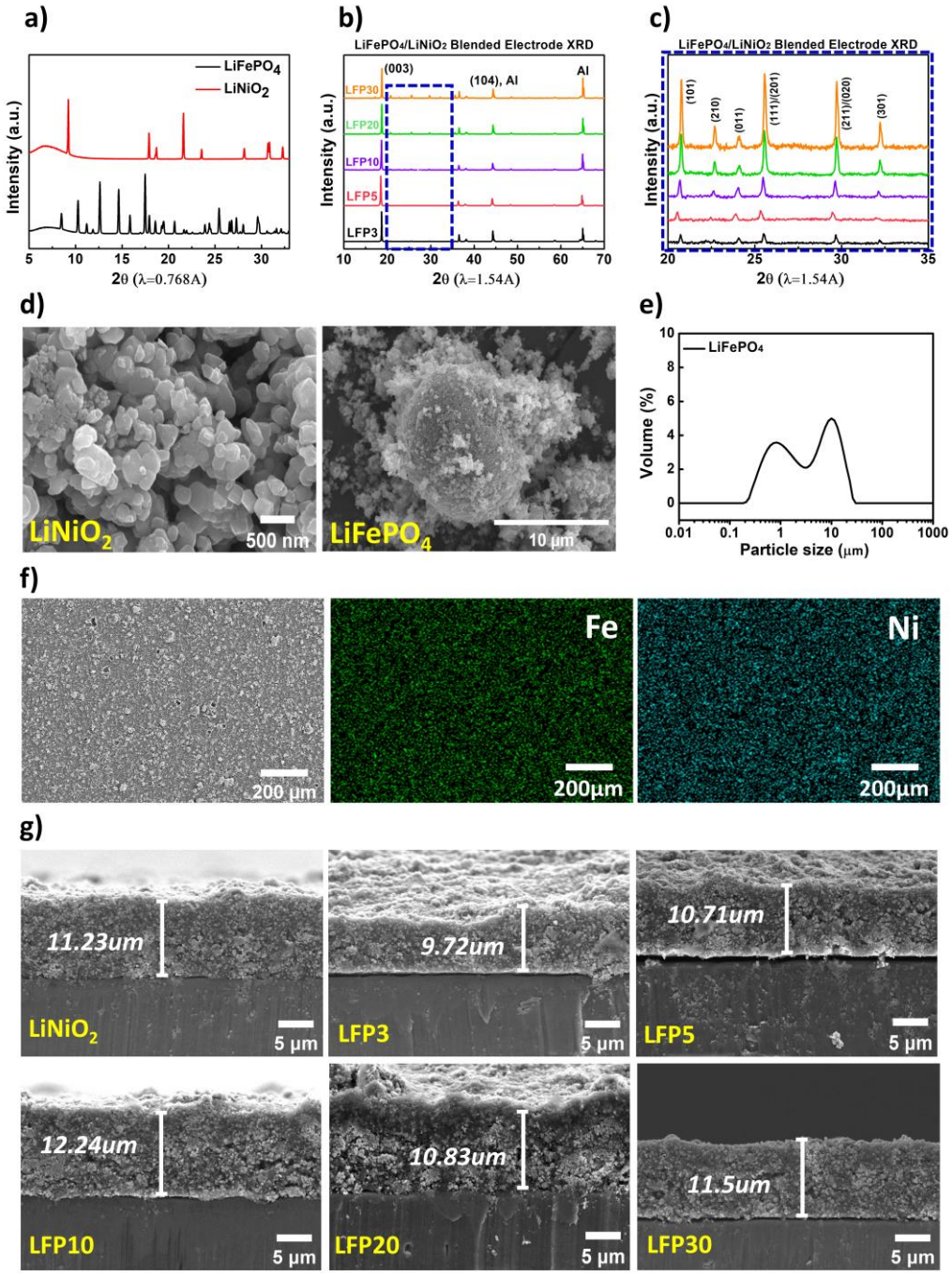

Fig. S3. a) Synchrotron XRD patterns of $LiFePO_4$, $LiNiO_2$. b) XRD patterns of LFP3, LFP5, LFP10, LFP20, and LFP30 blended electrodes and c) its enlarged view of 20° - 35° (2θ degree). d) SEM images of $LiNiO_2$ and $LiFePO_4$ particles. e) Particle size distribution of $LiFePO_4$. f) SEM images and energy-dispersive X-ray spectroscopy (EDX) mapping images (Fe, Ni element) of LFP30 blended electrodes (top view). EDX results indicate that the active materials ($LiNiO_2$ and $LiFePO_4$) are distributed uniformly. g) Cross-sectional SEM images of $LiNiO_2$ electrode, LFP3, LFP5, LFP10, LFP20, and LFP30 blended electrodes, indicating similar electrode loading level across the electrodes.

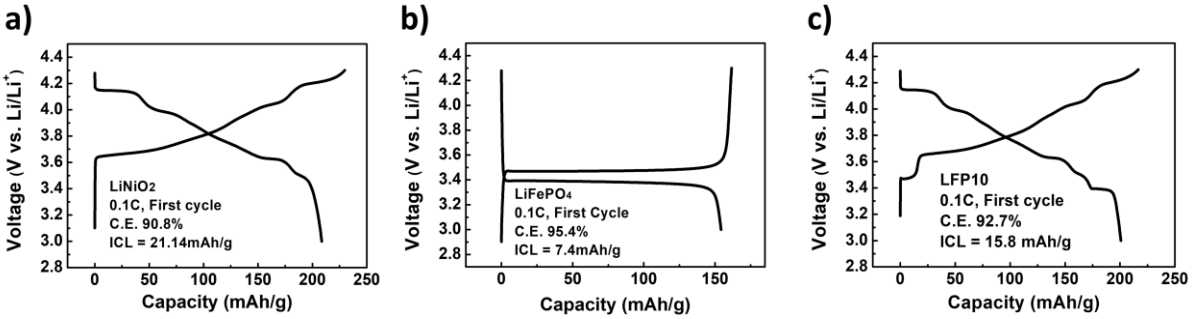

Fig. S4. Voltage *vs.* capacity curves of a) $LiNiO_2$, b) $LiFePO_4$, and c) LFP10 during the first cycle at 0.1C with the voltage range of 3.0 V – 4.3 V.

Table S1. ICL values and Initial Coulombic efficiencies of $LiNiO_2$ and $LiFePO_4$, and LFP10 from Fig. S4. (Experimental value and linearly combined value).

	$LiNiO_2$	**$LiFePO_4$**	**Linearly combined value of LFP10**	**Experimental value of LFP10**
ICL (mAh g^{-1})	21.1	7.4	19.7	15.8
Coulombic Efficiency (%)	90.8	95.4	91.2	92.7
Linear Combination	A	B	0.9A + 0.1B	-

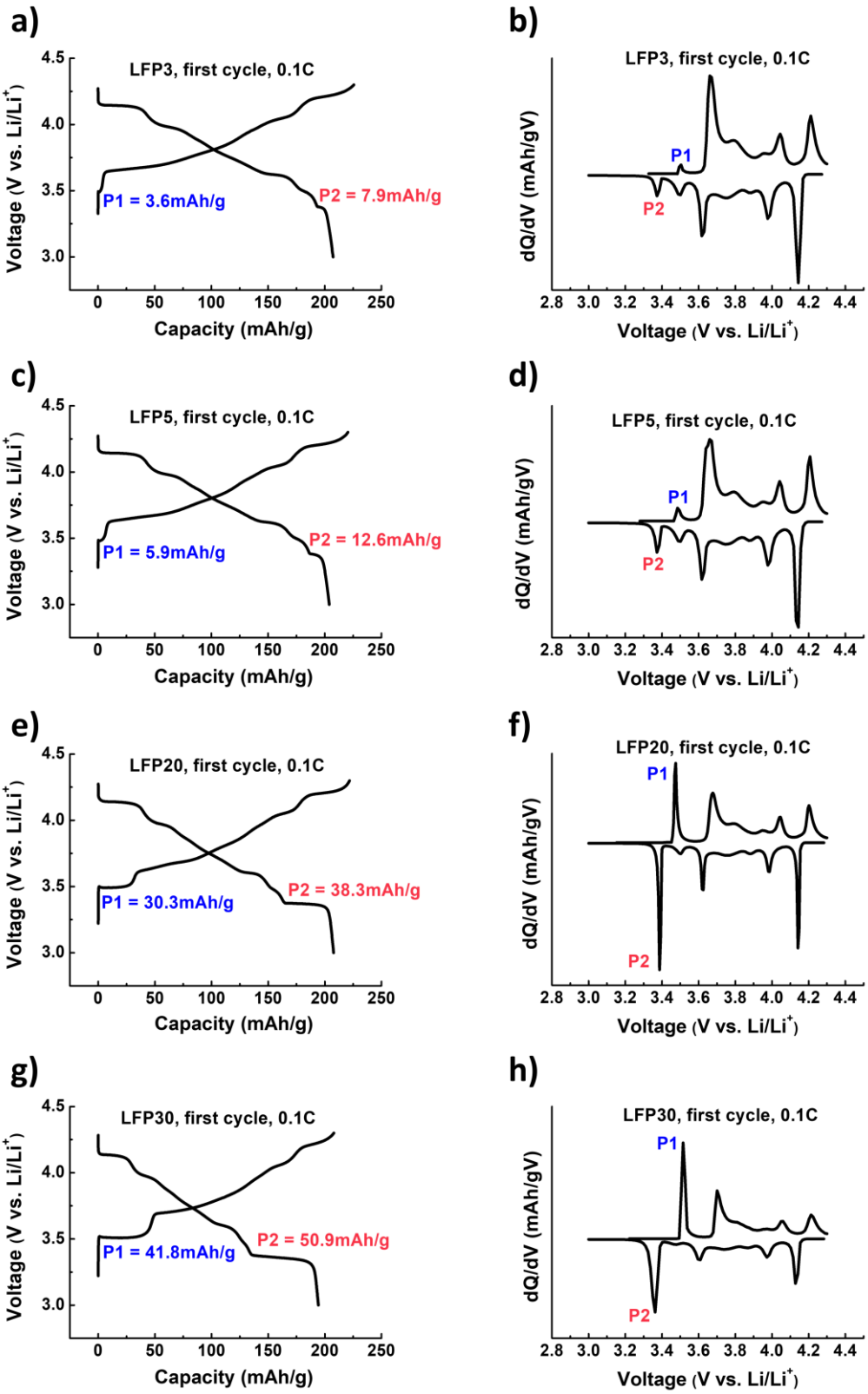

Fig. S5. Voltage *vs.* capacity curves of a) LFP3, c) LFP5, e) LFP20, g) LFP30, and corresponding differential capacity *vs.* voltage curves of b) LFP3, d) LFP5, f) LFP20 and h) LFP30 during first cycle at 0.1C with the voltage range of 3.0 V – 4.3 V.

Table S2. ICL, initial coulombic efficiencies, and the extent of internal Li ion transfer of $LiNiO_2$, LFP3, LFP5, LFP10, LFP20, and LFP30 blended electrodes at 0.1C.

	$LiNiO_2$	**LFP3**	**LFP5**	**LFP10**	**LFP20**	**LFP30**
ICL (mAh g^{-1})	21.1	18.3	16.5	15.8	14.1	13.6
Initial coulombic efficiency (%)	90.8	91.8	92.4	92.7	93.4	93.4
The extent of internal Li ion transfer: Capacity difference between P2 and P1 (mAh g^{-1})	0	4.3	6.7	7.9	8	9.1

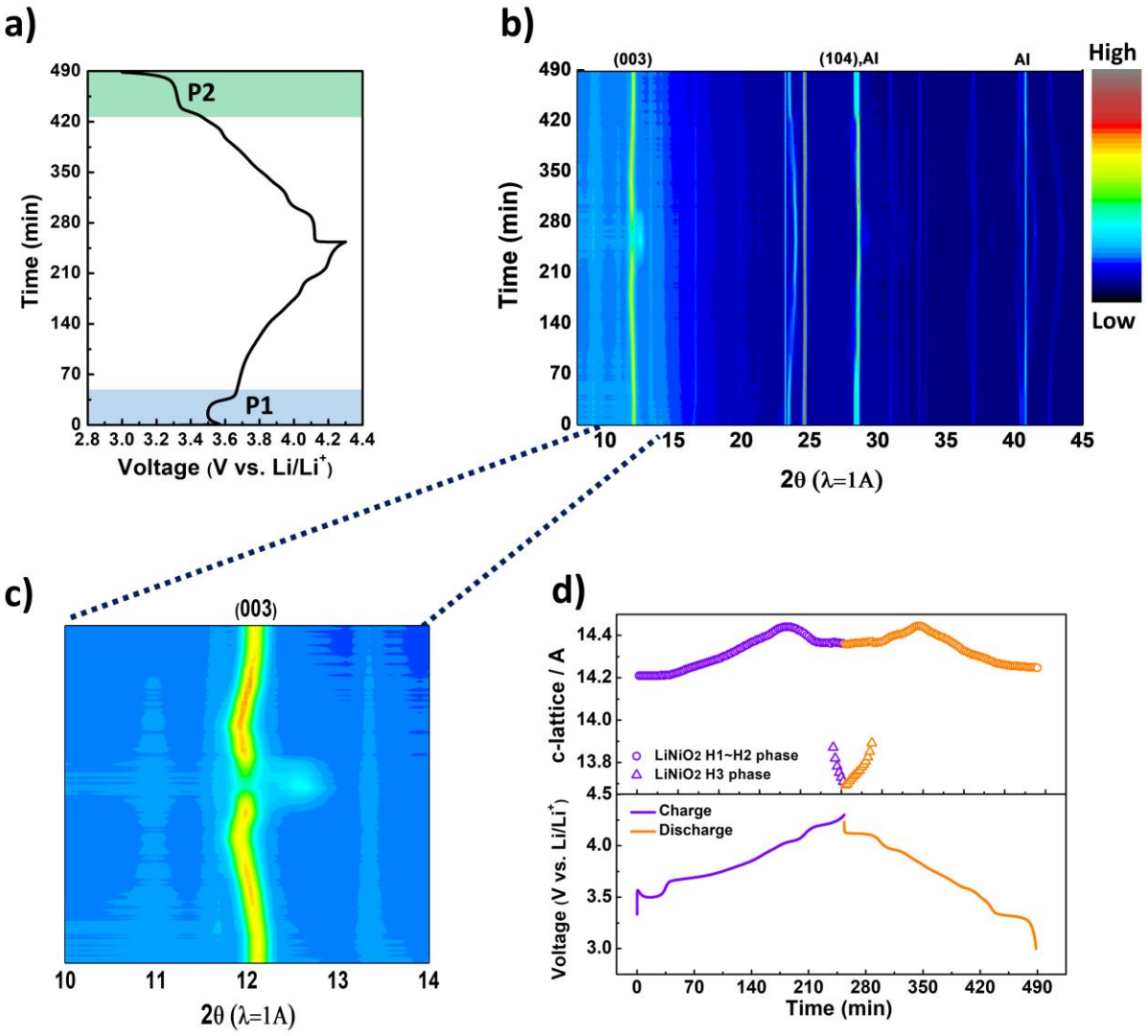

Fig. S6. a) Time *vs.* voltage curves of LFP20 during the first cycle at 0.2C with the voltage range of 3.0 V – 4.3 V, obtained during synchrotron in-situ XRD measurement. b) Corresponding XRD peak evolution as contour plot in the overall 2θ range (8° - 45°). c) Selected 2θ region (10° - 14°) of panel b), indicating the (003) reflection of $LiNiO_2$. d) Evolution of the c-axis lattice parameter of $LiNiO_2$ and corresponding voltage profile of the LFP20 electrode.

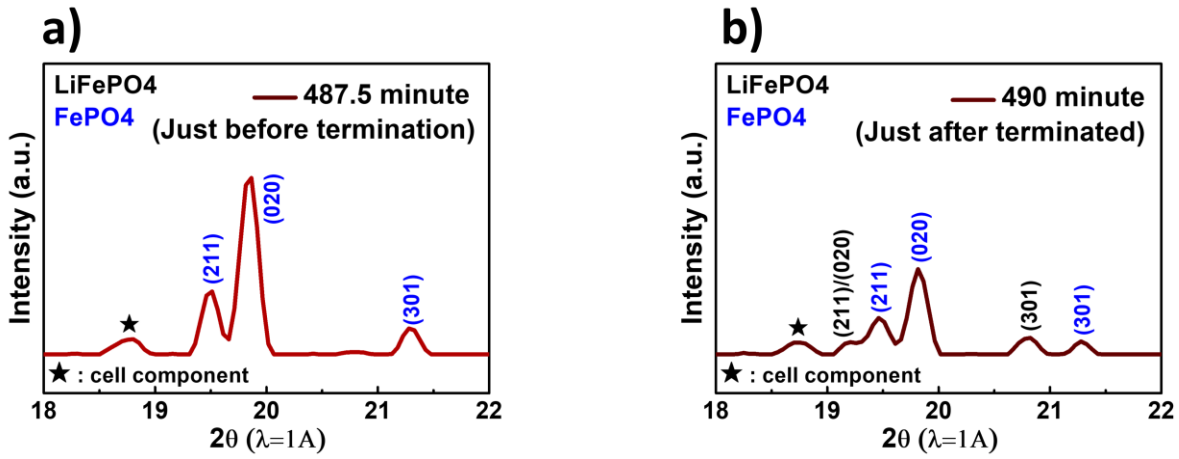

Fig. S7. The final two in-situ XRD patterns at the end of discharge (Fig. 3c) are shown: a) just before the termination and b) just after the test terminated.

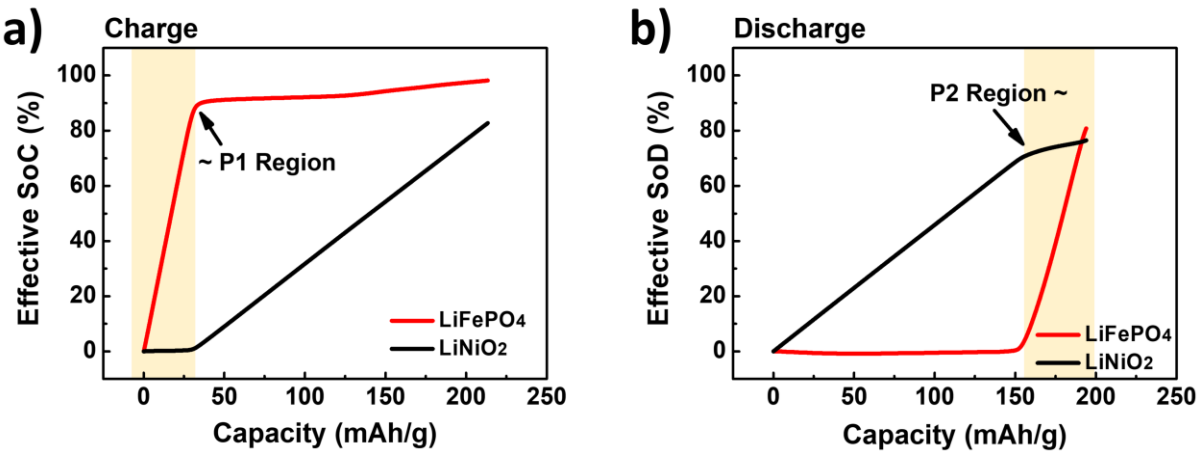

Fig. S8. Effective state of charge (SOC) and state of discharge (SOD) profiles of $LiFePO_4$ and $LiNiO_2$ as a function of the specific capacity (mAh g^{-1}) of the model electrochemical cell (M_LFP20) during the first cycle at 0.2C. a) Charge process. b) Discharge process. The effective SOC and SOD for each active material were calculated from the deconvoluted current–capacity profiles shown in Fig. 5a–b of the manuscript, based on the theoretical capacity of each active material in the M_LFP20.

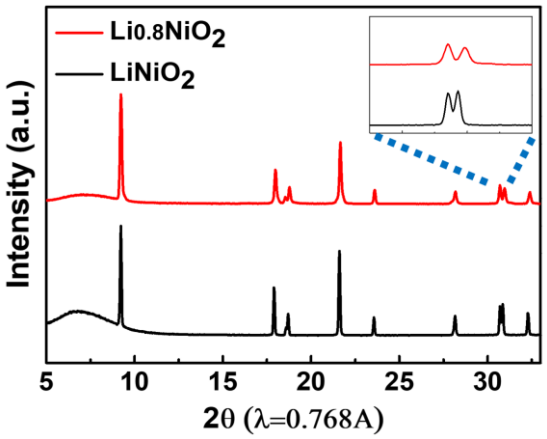

Fig. S9. Synchrotron XRD patterns of pristine $LiNiO_2$, and chemically delithiated $Li_{0.8}NiO$.

Table S3. ICP-OES results and AAS results of chemically delithiated $Li_{0.8}NiO_2$ and $LiNiO_2$.

Sample	Element	ICP-OES Result (ppm)	AAS Result (ppm)	Mol ratio
$LiNiO_2$	Li	-	73170	1.054
	Ni	600000	-	1.022
$Li_{0.8}NiO_2$	Li	-	55940	0.806
	Ni	591900	-	1.008

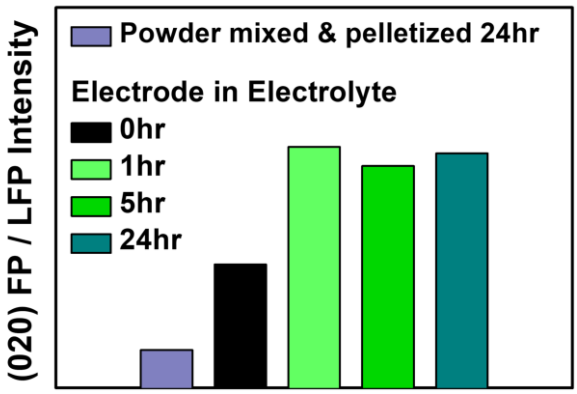

Fig. S10. Intensity ratio of $FePO_4$ (020) to $LiFePO_4$ (211)/(020) observed in Fig. 6b-c.

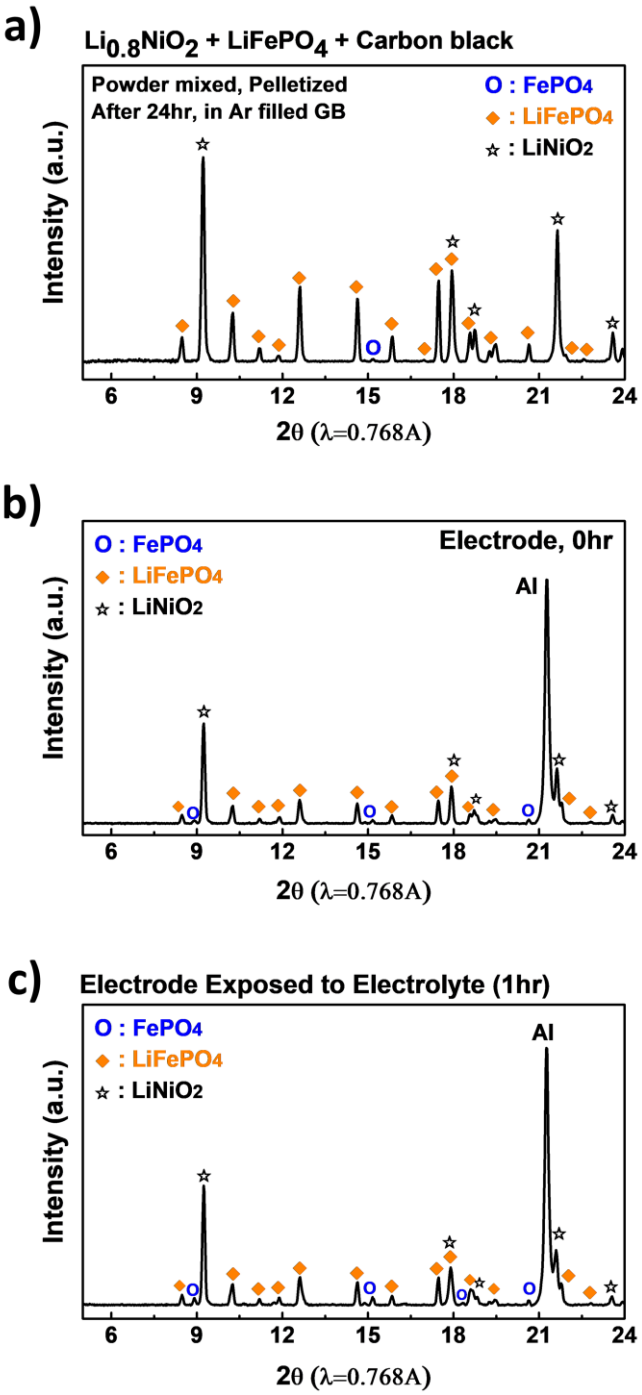

Fig. S11. Synchrotron XRD results at overall 2θ regions (5° - 24°) for a mixture of $LiFePO_4$ and chemically delithiated $Li_{0.8}NiO_2$ (50:50 wt.%) under various conditions. a) Each material is mixed together in agate mortar and pelletized, maintaining for 24hr in glove box. Each material is fabricated into a composite electrode, which is then relaxed in electrolyte for b) 0 hour, c) 1 hour. The composite electrodes consist of active materials ($LiFePO_4$ and chemically delithiated $Li_{0.8}NiO_2$ at a 50:50 wt.% ratio), carbon black, and PVDF binder in a weight ratio of 75:20:5.

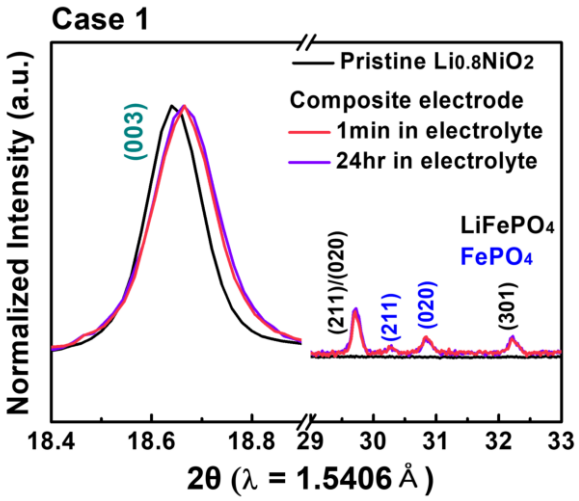

Fig. S12. XRD patterns of a composite electrode comprising active materials ($LiFePO_4$ and chemically delithiated $Li_{0.8}NiO_2$ at a 50:50 wt.% ratio), carbon, and PVDF in a weight ratio of 75:20:5, in two different states: after 1-minute relaxation (red) and after 24-hour relaxation (purple) in liquid electrolyte. These are compared with pristine $Li_{0.8}NiO_2$ (black). XRD patterns are shown for selected 2θ regions: 18.4° – 19.0°, corresponding to the (003) reflection of $Li_{0.8}NiO_2$, and 29° – 33°, corresponding to the (211) and (020) reflections indicating $FePO_4$ formation in the composite electrode.

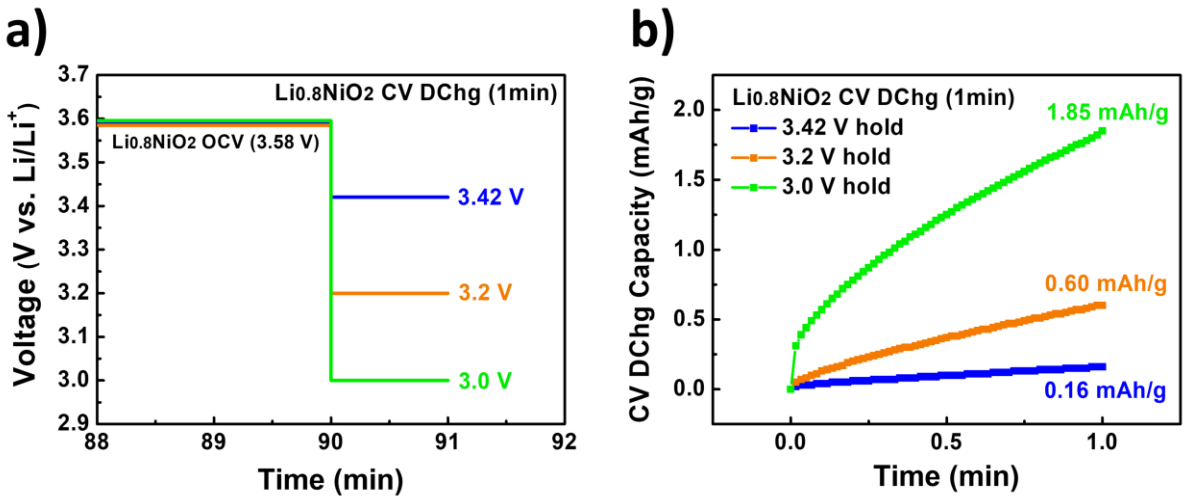

Fig. S13. a) Voltage vs. time profiles and b) capacity vs. time profiles of $Li_{0.8}NiO_2$ during a 1-minute constant voltage hold at 3.42 V, 3.20 V, and 3.00 V.

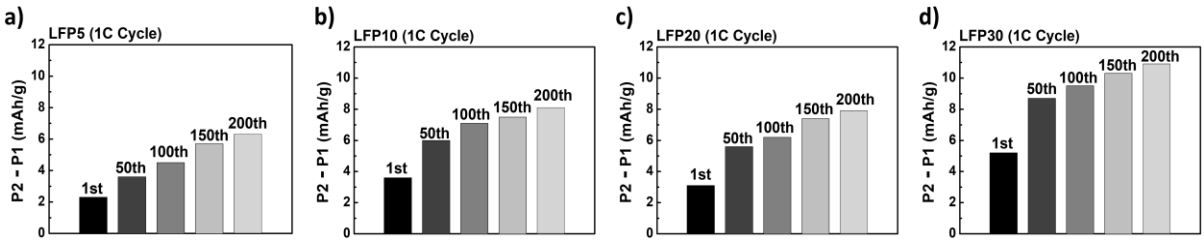

Fig. S14. Difference in capacities transferred at P2 and P1 for a) LFP5, b) LFP10, c) LFP20, and d) LFP30 at the 1st, 50th, 100th, 150th, and 200th cycles during the cycle retention test at 1C rate (voltage range: 3.0 V – 4.3 V).

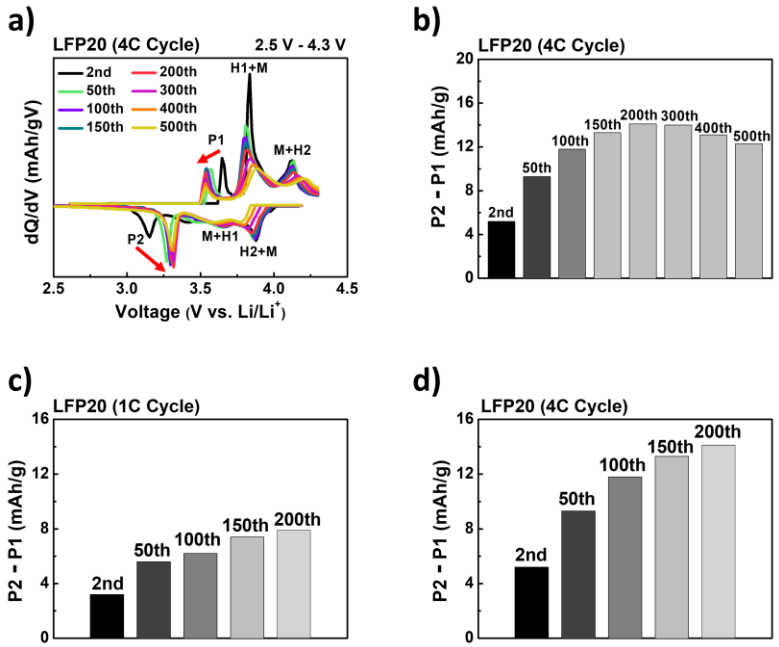

Fig. S15. a) Differential capacity (dQ/dV) *vs.* voltage curves of LFP20 at the 2nd, 50th, 100th, 150th, 200th, 300th, 400th, and 500th cycles during the 500-cycle retention test at 4C (voltage range: 2.5 V–4.3 V). b) Difference in capacities transferred at P2 and P1 (P2 – P1) of LFP20 at the 2nd, 50th, 100th, 150th, 200th, 300th, 400th, and 500th cycles during the retention test for 500 cycles at 4C. c) P2 – P1 capacity differences for LFP20 during the 1C retention test at the 2nd, 50th, 100th, 150th, and 200th cycles (identical to Fig. S14c). d) P2 – P1 capacity differences at 4C, extracted from the initial 200 cycles of the 500-cycle dataset shown in panel b, for direct comparison with 1C results in panel c.

Fig. S15a shows the evolution of the dQ/dV peaks as a function of cycle number for LFP20 during the 500-cycle retention test at 4C, presented as a representative example. The extent of internal Li-ion transfer in LFP20—quantified by the capacity difference between the P1 and P2 plateaus—is plotted as a function of cycle number in Fig. S15b. The results show that this difference increased with cycling up to 300 cycles and remained substantial through 500 cycles, indicating that internal Li-ion transfer was sustained throughout the 500-cycles and contributed to mitigating capacity degradation.

Furthermore, when comparing the extent of internal Li-ion transfer in LFP20 at 1C (Fig. S15c) and 4C (Fig. S15d) over 200 cycles, the effect was more pronounced at 4C. This is likely due to the accelerated degradation of $LiNiO_2$ at higher C-rates, which leads to a more Li-deficient state in $Li_{1-x}NiO_2$ and increases the potential difference with $LiFePO_4$, thereby enhancing the thermodynamic driving force for internal Li-ion transfer.

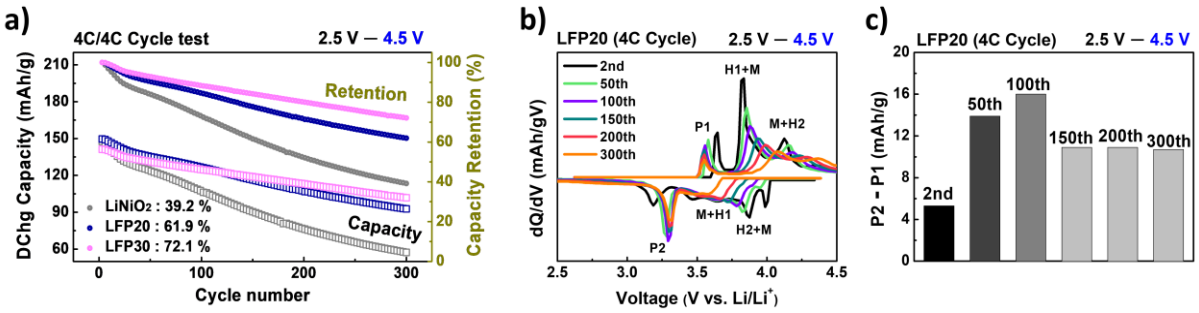

Fig. S16. a) Specific discharge capacity (Left - y axis, open squares) and capacity retention (Right - y axis, filled circles) *vs*. cycle number curves during 300 cycles at 4C for $LiNiO_2$, LFP20, and LFP30. Voltage range: 2.5 V — 4.5 V. b) Differential capacity (dQ/dV) *vs.* voltage curves of LFP20 at the 2^{nd}, 50^{th}, 100^{th}, 150^{th}, 200^{th}, and 300^{th} cycles during the retention test at 4C. c) Difference in capacities transferred at P2 and P1 of LFP20 at the 2^{nd}, 50^{th}, 100^{th}, 150^{th}, 200^{th}, and 300^{th} cycles during the retention test at 4C.

Fig. S16a compares the cycling retention performance of various blended electrodes at 4C under a high cutoff voltage condition (2.5 V – 4.5 V). The results indicate that electrodes with higher $LiFePO_4$ content exhibited superior long-term stability. This enhanced performance allowed the capacities of most blended electrodes to eventually surpass that of the pure $LiNiO_2$ electrode after several cycles.

Fig. S16b shows the evolution of the dQ/dV peaks for LFP20 as a function of cycle number. Based on these plots, the extent of internal Li-ion transfer in LFP20—quantified by the capacity difference between the P2 and P1 plateaus (P2 – P1)—was calculated and plotted as a function of cycle number in Fig. S16c. The results show that the extent of internal Li-ion transfer continued to increase up to 100 cycles under the 4.5 V condition, exceeding that observed at 4.3 V (Fig. S15b). However, this trend did not persist beyond 100 cycles, likely due to degradation of the $LiFePO_4$ phase at high cutoff voltages, as evidenced by the continuous decline in the dQ/dV peak corresponding to the P1 plateau (Fig. S16b). Additionally, $LiNiO_2$ may experience severe structural degradation and loss of electrochemical activity under prolonged 4.5 V cycling, which cannot be fully compensated by the internal Li-ion transfer mechanism.

Nevertheless, because a substantial P2 – P1 value remains even after 150 cycles, we conclude that internal Li-ion transfer continues to play an important role in mitigating capacity degradation, even under high-voltage operation.

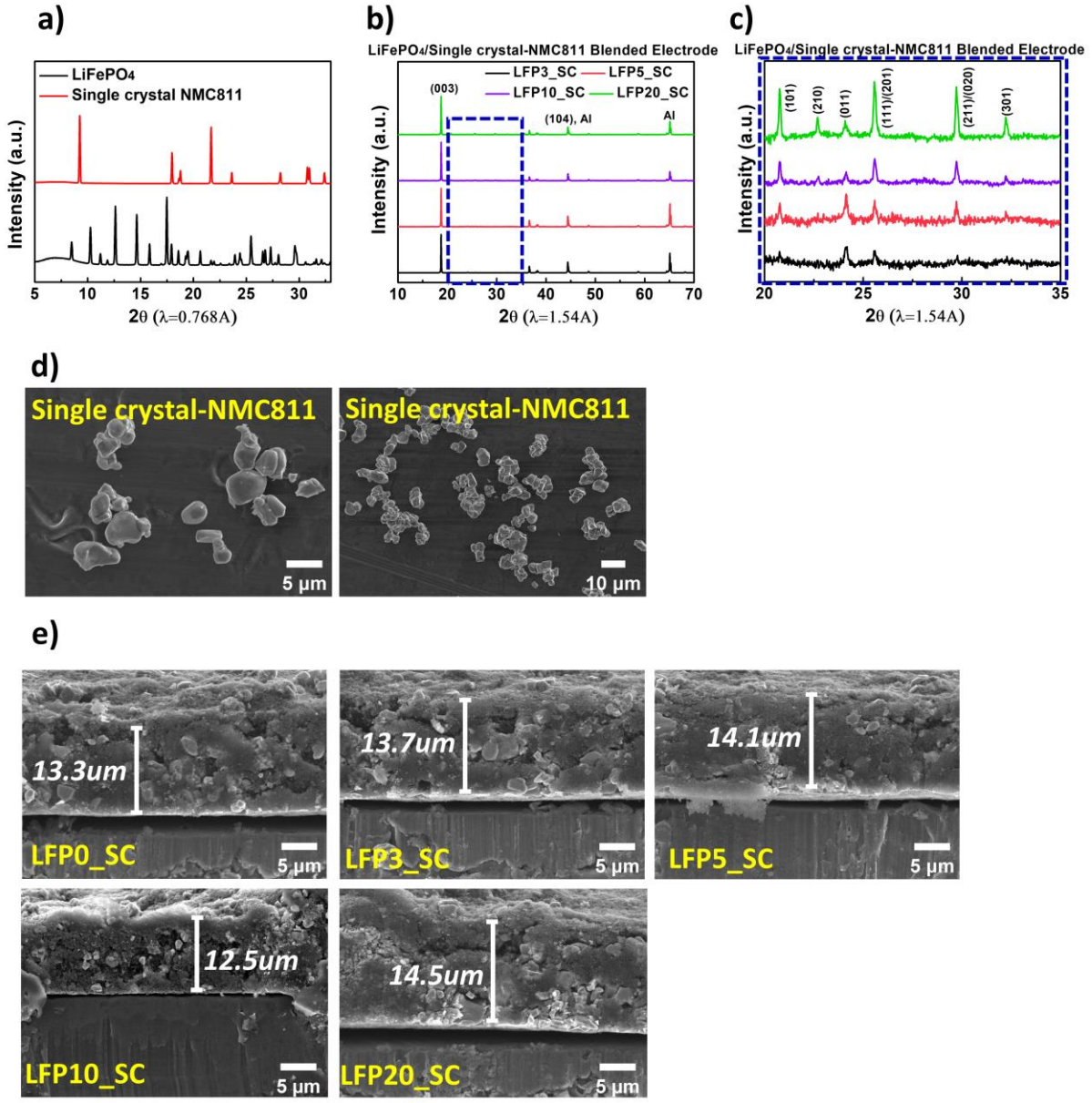

Fig. S17. a) Synchrotron XRD patterns of $LiFePO_4$ and single crystal NMC811. b) XRD patterns of LFP3_SC, LFP5_SC, LFP10_SC, and LFP20_SC blended electrodes and c) its enlarged view of 2θ range (20° - 35°), highlighted by the blue dashed square. d) SEM images of SC-NMC811 particles. e) Cross-sectional SEM images of LFP0_SC, LFP3_SC, LFP5_SC, LFP10_SC, and LFP20_SC blended electrodes, indicating similar electrode loading level across the electrodes.

Table S4. ICL, initial coulombic efficiencies, and the extent of internal Li ion transfer of LFP0_SC, LFP3_SC, LFP5_SC, LFP10_SC, LFP20_SC, and LFP30_SC blended electrodes at 0.1C.

	LFP0_SC	**LFP3_SC**	**LFP5_SC**	**LFP10_SC**	**LFP20_SC**	**LFP30_SC**
ICL (mAh g^{-1})	28.9	26.1	24.4	24.6	21.5	19.2
Initial coulombic efficiency (%)	86.7	87.8	88.5	88.5	89.7	90.1
The extent of internal Li ion transfer: Capacity difference between P2 and P1 (mAh g^{-1})	0	3.9	5.2	6.8	7.1	8.2

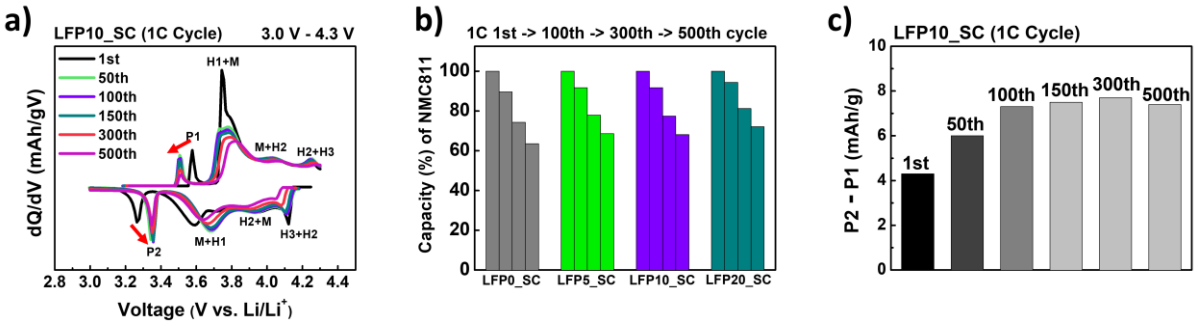

Fig. S18. a) Differential capacity (dQ/dV) *vs.* voltage curves of LFP10_SC at the 1st, 50th, 100th, 150th, 300th, and 500th cycles during the retention test for 500 cycles at 1C. b) Capacity change of single crystal NMC811 in each sample (LFP0_SC, LFP5_SC, LFP10_SC, and LFP20_SC) at the 1st, 100th, 300th, and 500th cycles during the retention test for 500 cycles at 1C. c) Difference in capacities transferred at P2 and P1 of LFP10_SC at 1st, 50th, 100th, 150th, 300th, and 500th cycles during the retention test for 500 cycles at 1 C. Voltage range: 3.0 V – 4.3 V.

Fig. S18a shows the evolution of the dQ/dV peaks as a function of cycle number for LFP10_SC, presented as a representative example. Based on these plots, the capacity contribution from the single-crystal NMC811 component in LFP10_SC was extracted and plotted in Fig. S18b, along with a comparison to that of LFP0_SC (pure single-crystal NMC811 electrode). The results clearly show that the capacity of the single-crystal NMC811 component in LFP10_SC gradually decreases at a rate similar to that of the LFP0_SC. This trend was also observed in LFP5_SC and LFP20_SC.

The change in the extent of internal Li-ion transfer in LFP10_SC—quantified by the capacity difference between the P1 and P2 plateaus—is plotted as a function of cycle number in Fig. S18c. The results show that this difference gradually increased with cycling up to 300 cycles and remained substantial through 500 cycles, suggesting that internal Li-ion transfer was sustained throughout the 500-cycles, thereby contributing to the mitigation of capacity degradation.

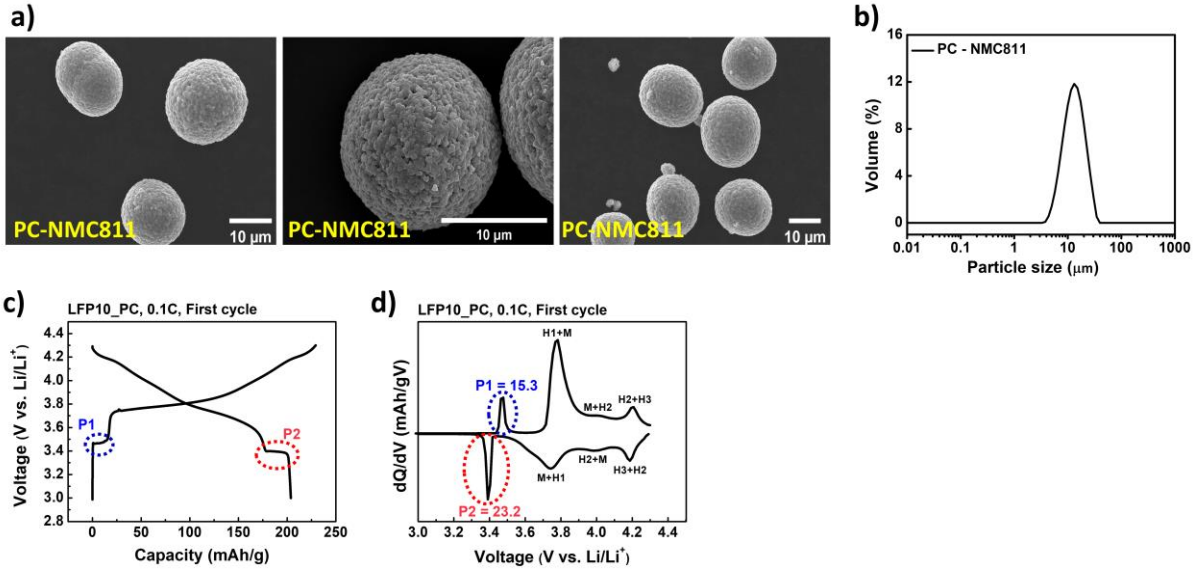

Fig. S19. a) SEM images and b) particle size distribution of polycrystalline-NMC811 (PC-NMC811). c) Voltage *vs.* capacity curves of LFP10_PC during the first cycle at 0.1 C, and d) its differential capacity (dQ/dV) *vs.* voltage curves with the voltage range of 3.0 V – 4.3 V.

Table S5. ICL, initial coulombic efficiencies, and the extent of internal Li ion transfer of LFP0_PC, LFP3_PC, LFP5_PC, LFP10_PC, LFP20_PC, and LFP30_PC blended electrodes at 0.1 C.

	LFP0_PC	**LFP3_PC**	**LFP5_PC**	**LFP10_PC**	**LFP20_PC**	**LFP30_PC**
ICL (mAh g^{-1})	31.9	29.1	28.1	25.5	22.5	18.3
Initial coulombic efficiency (%)	85.7	86.6	87.4	88.8	89.7	91.2
The extent of internal Li ion transfer: Capacity difference between P2 and P1 (mAh g^{-1})	0	3.9	6.2	7.9	8.3	8.6

We prepared a commercial polycrystalline NMC811 cathode (referred to as LFP0_PC), purchased from Shandong Gelon Lib Co., Ltd. We prepared five polycrystalline NMC811/$LiFePO_4$ blended electrodes with varying $LiFePO_4$ content (3%, 5%, 10%, 20%, and 30% by weight), referred to as LFP3_PC, LFP5_PC, LFP10_PC, LFP20_PC, and LFP30_PC.

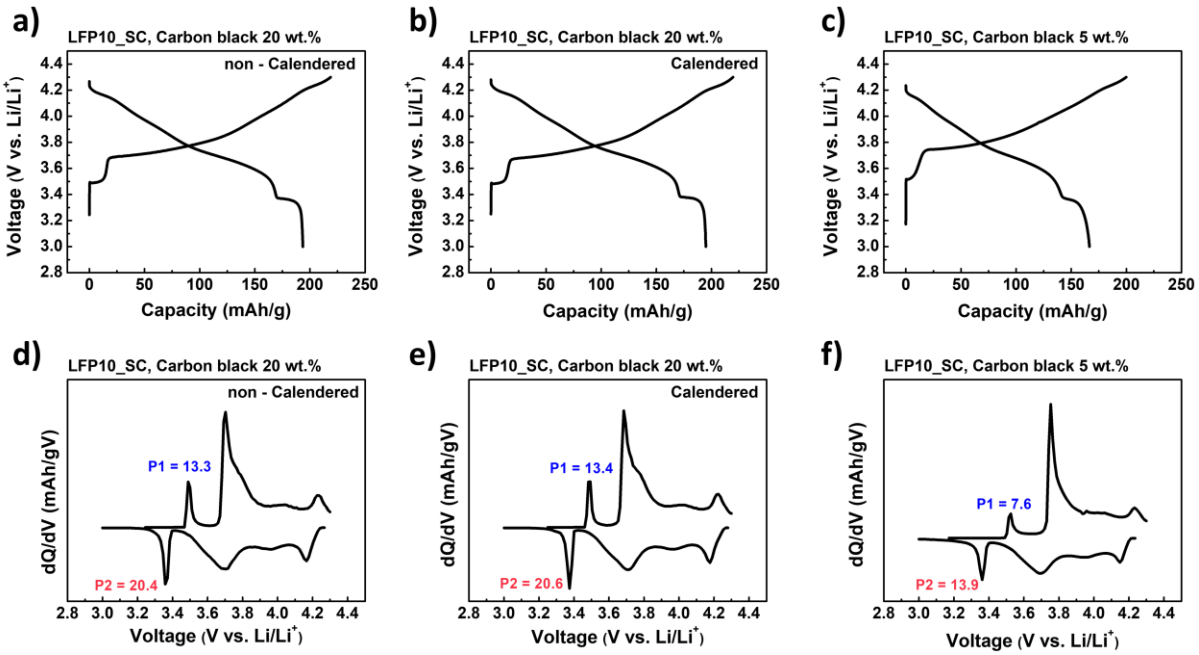

Fig. S20. a-c) Voltage vs. capacity profiles and d–f) corresponding differential capacity (dQ/dV) curves of LFP10_SC electrodes during the first cycle at 0.1C (voltage range: 3.0–4.3 V), measured under different electrode processing conditions. a, d) Non-calendered electrode composed of 75 wt.% active material, 20 wt.% carbon black, and 5 wt.% PVDF binder. b, e) Calendered electrode composed of 75 wt.% active material, 20 wt.% carbon black, and 5 wt.% PVDF binder. c, f) Non-calendered electrode with a higher active material loading (90 wt.%) and reduced carbon black content (5 wt.%), with 5 wt.% PVDF binder.

Table S6. Charge and discharge capacities, initial coulombic efficiencies, and the extent of internal Li ion transfer of LFP10_SC blended electrodes under different electrode processing conditions. These values were extracted from Fig. S20.

	a) LFP10_SC, non-calendered	**b) LFP10_SC, calendered**	**c) LFP10_SC, carbon black 5wt.%**
Electrode composition	75 wt.% active material, 20 wt.% carbon black, and 5 wt.% PVDF binder	75 wt.% active material, 20 wt.% carbon black, and 5 wt.% PVDF binder	90 wt.% active material, 5 wt.% carbon black, and 5 wt.% PVDF binder.
Charge capacity (mAh g^{-1})	218.78	219.63	199.92
Discharge capacity (mAh g^{-1})	193.64	194.98	166.56
Initial coulombic efficiency (%)	88.50	88.78	83.31
The extent of internal Li ion transfer: Capacity difference between P2 and P1 (mAh g^{-1})	7.1	7.2	6.3

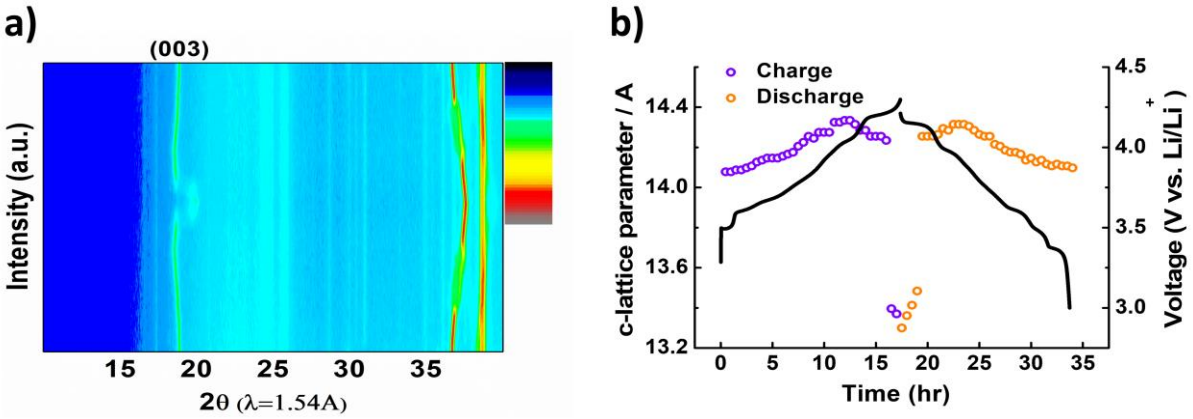

Fig. S21. a) In-situ XRD results as contour plot of intensity for LFP10, during the first cycle at 0.05C at overall 2θ regions (10° - 40°), and b) corresponding c-lattice change of $LiNiO_2$ with voltage curves in the voltage range of 3.0 V – 4.3 V.